

First-principles study of type-I and type-VIII $\text{Ba}_8\text{Ga}_{16}\text{Sn}_{30}$ clathrates

Yasushi Kono,^{1,2,a)} Nobuyuki Ohya,¹ Takashi Taguchi,¹ Koichiro Suekuni,³
Toshiro Takabatake,³ Setsuo Yamamoto,² and Koji Akai⁴

¹DENSO Corporation Research Laboratories, Minamiyama, 500-1, Komenogi, Nisshin 470-0111, Japan

²Graduate School of Science and Engineering, Yamaguchi University, Tokiwadai, 2-16-1,
Ube 755-8611, Japan

³Department of Quantum Matter, ADSM, Hiroshima University, Kagamiyama, 1-3-1,
Higashi-Hiroshima 739-8530, Japan

⁴Media and Information Technology Center, Yamaguchi University, Yoshida, 1677-1,
Yamaguchi 753-8511, Japan

(Received 23 December 2009; accepted 5 May 2010; published online 30 June 2010)

We calculated the electronic structures and the thermoelectric properties for type-I and type-VIII $\text{Ba}_8\text{Ga}_{16}\text{Sn}_{30}$ (BGS) clathrates. The band structures show that type-I and type-VIII BGS are indirect semiconductors with band gaps of 0.51 eV and 0.32 eV, respectively. The calculated Seebeck coefficient of *n*-type type-I BGS is higher than that of *n*-type type-VIII BGS because of the larger density of states in type-I at the bottom of the conduction band. This is in good agreement with the experimental results. We also calculated the electrical conductivity and thermal conductivity due to charge carriers. Estimated thermoelectric figure of merit, *ZT*, exceeds 1.0 for both types.

© 2010 American Institute of Physics. [doi:10.1063/1.3437252]

I. INTRODUCTION

Recently, group IV based clathrate compounds are attracting much attention as high performance thermoelectric materials from the perspective of “phonon glass and electron crystal”.^{1,2} This feature is brought from the unique crystal structure of clathrates. Clathrates are composed of several kinds of molecular cages enclosed with guest atom. These cages are also connected each other by face sharing. Therefore, host atoms construct a three-dimensional network of *sp*³ bonds. A guest atom in the host cage is loosely bound within the framework and causes anharmonic and localized atomic vibration. This localized atomic vibration is referred to as rattling. In spite of crystal, this rattling mode scatters thermal-conducting phonons effectively and causes glasslike low thermal conductivity. In many group IV based clathrates, the guest element is an alkali or an alkaline-earth metal. One of the typical group IV clathrates is $\text{Ba}_8\text{Ga}_{16}\text{Ge}_{30}$ which shows *ZT*=1.63 at 1100 K.³

Tin-based clathrates crystallize in several kinds of structures: type-I, type-III, and type-VIII.⁴ For example, $\text{Ba}_8\text{Ga}_{16}\text{Sn}_{30}$ (BGS) has two kinds of crystal structures, type-I⁵ and type-VIII.^{6,7} In both of those structures, the host atom is bonded with 4 neighbor atoms by the *sp*³ hybridizing orbital. Their local geometries are similar but their unit cell structures and crystal symmetries are different. Type-I structure is composed of two kinds of molecular cages surrounding guest atoms such as: X_{20} and X_{24} ($\text{X}=\text{Sn}$ or Ga). On the other hand, type-VIII structure is composed of only one kind of dodecahedral cage. Small empty spaces exist between each cage. This difference in the crystal structure is expected to affect thermal and thermoelectric properties. The thermoelectric properties of type-VIII BGS (BGS-VIII) have been measured by some authors in both of polycrystalline^{8,9} and

single crystalline samples.^{10,11} Single crystalline samples of type-I BGS (BGS-I) were prepared and their thermal properties were measured.¹² Recently, Suekuni *et al.*¹³ reported thermoelectric properties of both types of BGS at temperatures below 300 K. In the present study, we theoretically investigate the electronic structure and thermoelectric properties of both types of BGS. It should be noted that similar calculations have been reported for BGS-VIII.^{14–17} The band structure of BGS-VIII has been calculated by pseudopotential method and this result indicated a metallic nature. This is inconsistent with the observed semiconducting behavior.^{18,8} The thermoelectric properties of BGS have been calculated for only the BGS-VIII.¹⁹ The goal in this study is to discuss the potential of both types of BGS as high performance thermoelectric materials. In Sec. II we show the computational methods of band structure and thermoelectric properties briefly, and in Sec. III we discuss the calculated results, i.e., band structure and thermoelectric properties in both types of BGS.

II. COMPUTATIONAL DETAILS

A. Band structure calculation

We calculated the electronic structure of BGS by using the full potential linearized augmented plane wave (FLAPW) method based on the density-functional theory.²⁰ The following values were used for the muffin-tin radii and the plane wave cutoff: $R_{\text{mt}}(\text{Ba})=3.0$ a.u., $R_{\text{mt}}(\text{Ga})=2.2$ a.u., $R_{\text{mt}}(\text{Sn})=2.2$ a.u., $R_{\text{mt}} K_{\text{max}}=7$. In the self-consistent field calculation, 516 k-sampling points were taken in the first Brillouin zone. For the exchange correlation energy, Engel–Vosko’s parametrized potential within the generalized gradient approximation (EV-GGA) was used.²¹ The lattice parameters were obtained by x-ray diffraction analysis, and then the lattice constants for BGS-I and BGS-VIII were 11.69 Å and 11.59 Å, respectively. As for Ga configuration in the host

^{a)}Electronic mail: m502wd@yamaguchi-u.ac.jp.

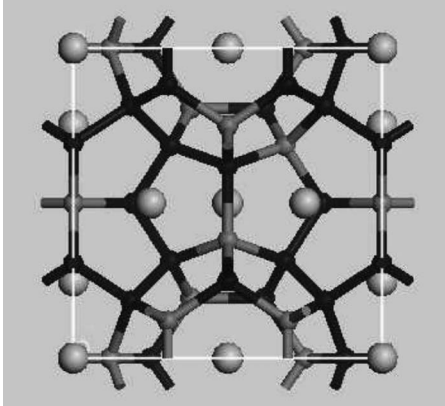
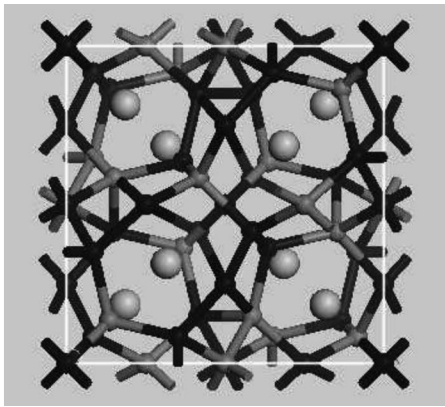
(a) type-I**(b) type-VIII**

FIG. 1. Crystal structure of BGS, (a) type-I structure and (b) type-VIII structure.

framework, there was some ambiguity. Blake *et al.* determined the atomic structure of type-I $\text{Ba}_8\text{Ga}_{16}\text{Ge}_{30}$ and $\text{Ba}_8\text{Ga}_{16}\text{Si}_{30}$ clathrates by minimizing the total energy using the first principle electronic structure calculation, discovering that Ga atoms avoid the nearest neighbor sitting each other.²² Therefore, in BGS-I, we used the unit cell model without Ga–Ga bonds. Similarly, we adopted a Ga sitting model for BGS-VIII which was consistent with fewer Ga–Ga bonds. As for Ga occupancy rate at each site, we used the experimental results done by Carrillo-Cabrera *et al.*⁷ In this work we applied the supercell approximation to take into account the Ga substitution in the host framework, and then the supercell was a unit cell of each BGS clathrate structures. The crystal models of each BGS are shown in Fig. 1.

B. Thermoelectric properties

We calculated transport properties by the semiclassical transport theory. By using the linearized Boltzmann equation with the relaxation time approximation, Seebeck coefficient α , electric conductivity σ , and electronic thermal conductivity κ_e are given as

$$\alpha = \frac{e}{3T\sigma} \int d\varepsilon \left(-\frac{\partial f}{\partial \varepsilon} \right) \rho(\varepsilon) \tau(\varepsilon) v(\varepsilon)^2 (\varepsilon - \mu), \quad (1)$$

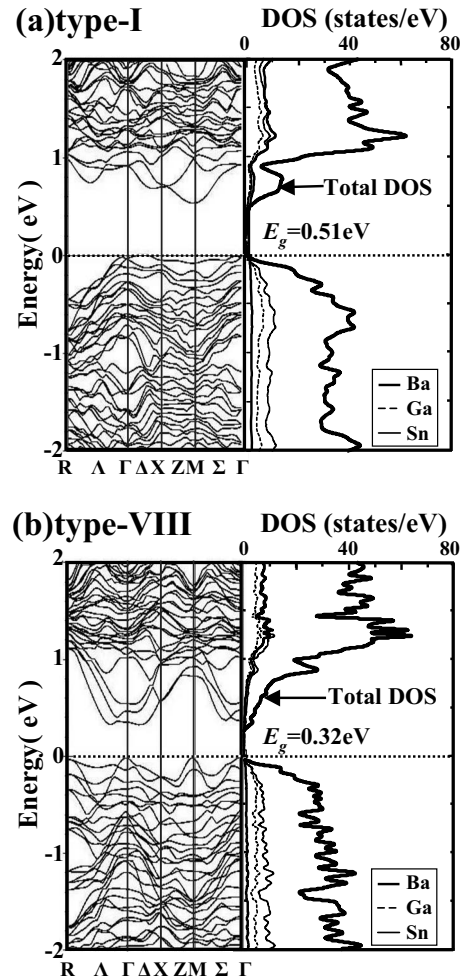


FIG. 2. The band structure and DOS for BGS, (a) type-I and (b) type-VIII. The dotted line denotes the Fermi level.

$$\sigma = \frac{e^2}{3} \int d\varepsilon \left(-\frac{\partial f}{\partial \varepsilon} \right) \rho(\varepsilon) \tau(\varepsilon) v(\varepsilon)^2, \quad (2)$$

$$\kappa_e = \frac{1}{3T} \int d\varepsilon \left(-\frac{\partial f}{\partial \varepsilon} \right) \rho(\varepsilon) \tau(\varepsilon) v(\varepsilon)^2 (\varepsilon - \mu)^2, \quad (3)$$

where $\rho(\varepsilon)$ is the density of states (DOS), $\tau(\varepsilon)$ is the relaxation time, $f(\varepsilon)$ is the Fermi distribution function, μ is the chemical potential, and $v(\varepsilon)$ is the carrier velocity, respectively. Then $v(\varepsilon)$ is given as

$$\rho(\varepsilon) v(\varepsilon)^2 = \sum_{nk} \delta(\varepsilon - \varepsilon_{nk}) \left| \langle nk | \frac{\hat{\mathbf{P}}}{m_0} | nk \rangle \right|^2. \quad (4)$$

Here, $\hat{\mathbf{P}}$ is the momentum operator, m_0 is the bare electron mass, while $|nk\rangle$ and ε_{nk} are the electronic state and the energy of the n th band at the wave number \mathbf{k} , respectively. In the present calculation, the energy dependence of $\tau(\varepsilon)$ is neglected: $\tau(\varepsilon) = \tau$. The relaxation time τ in Eq. (1) is canceled out between σ in the denominator and the numerator. Thus, Seebeck coefficient α is independent of τ , and can be determined by the band structure. We assumed the rigid band scheme, i.e., the band structure does not change with doping carriers (electrons or holes). The dimensionless figure of merit ZT of thermoelectric material is obtained as

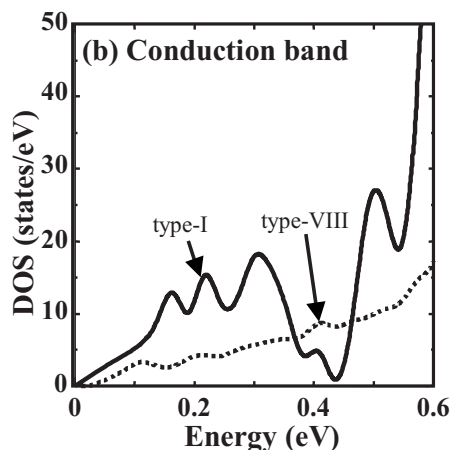
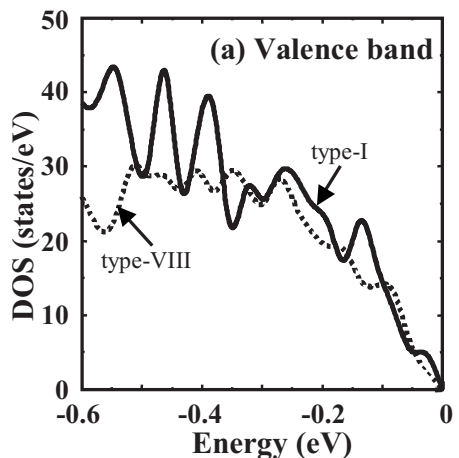


FIG. 3. Comparison with the DOS shape near the band edge between BGS-I and BGS-VIII: (a) valence band and (b) conduction band.

$$Z \cdot T = \frac{\alpha^2 \sigma}{\kappa_e + \kappa_L} T, \quad (5)$$

where, κ_L is the lattice thermal conductivity which is dealt with a constant value in this work. The details of the computational method are explained in Ref. 23.

III. RESULTS AND DISCUSSION

A. Electronic structure

The band structure and the DOS in BGS-I and BGS-VIII are shown in Figs. 2(a) and 2(b), respectively. The dotted lines denote the Fermi energy. The results show that BGS-I and BGS-VIII are indirect semiconductors with the energy gaps of 0.51 eV and 0.32 eV, respectively. The top of the valence band is relatively flat (near the Γ) and the bottom of the conduction band is positioned at the M point in BGS-I. In BGS-VIII, on the other hand, the top of the valence band is positioned at the M point and the bottom of the conduction band is positioned on the Δ axis. For both types, the valence band consists mainly of atomic orbitals of Ga and Sn, while the conduction band consists of the atomic orbitals of Ba as well as those of Ga and Sn. Figure 3 shows the shape of the band edge near the Fermi energy for the valence band and the conduction band. In each figure, the origin of the energy is at the top of the valence band and the bottom of the conduction band, respectively. In Fig. 3(a), the slope of the DOS

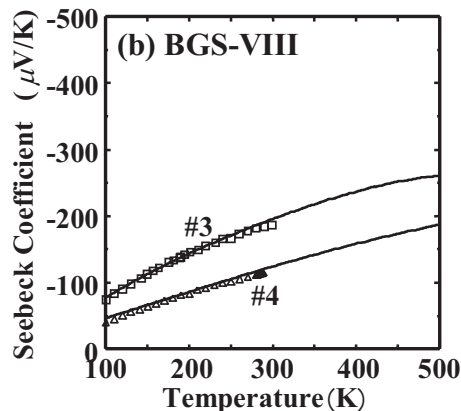
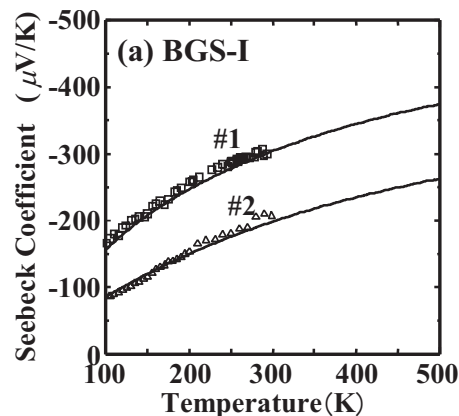


FIG. 4. Calculated Seebeck coefficient with n -type carriers: (a) BGS-I and (b) BGS-VIII. Solid lines denote calculated results. Open triangles and open squares are experimental results (Ref. 13).

near the valence-band edges are similar for both types, whereas in Fig. 3(b) the slope near the conduction-band edge for BGS-I is steeper than that of BGS-VIII. Therefore, it is expected that in p -type samples, Seebeck coefficient has similar magnitudes for both BGS-I and BGS-VIII, whereas in n -type Seebeck coefficient magnitude is larger BGS-I than BGS-VIII. We confirm this point in Sec. III B.

B. Thermoelectric properties

Suekuni *et al.*¹³ reported that the Seebeck coefficient of n -type BGS-I is higher than that of n -type BGS-VIII, and that n -type samples of BGS have similar carrier concentrations for both BGS-I and BGS-VIII. From only the experimental data this result is difficult to understand, because Seebeck coefficient depends strongly on the carrier concentration and the band structure.

The calculated Seebeck coefficient using Eq. (1) is presented in Fig. 4. The solid lines denote the calculations for n -type BGS-I (a) and BGS-VIII (b). Our calculation reproduces the temperature dependence of the Seebeck coefficients in the range of 100–300 K well, then the carrier concentrations used in the calculations have been determined to fit the experimental results. The estimated electron concentrations are shown in Table I. These results are comparable with those of the experimental values. These estimated carrier concentrations of Nos. 1 and 3 are smaller than those of

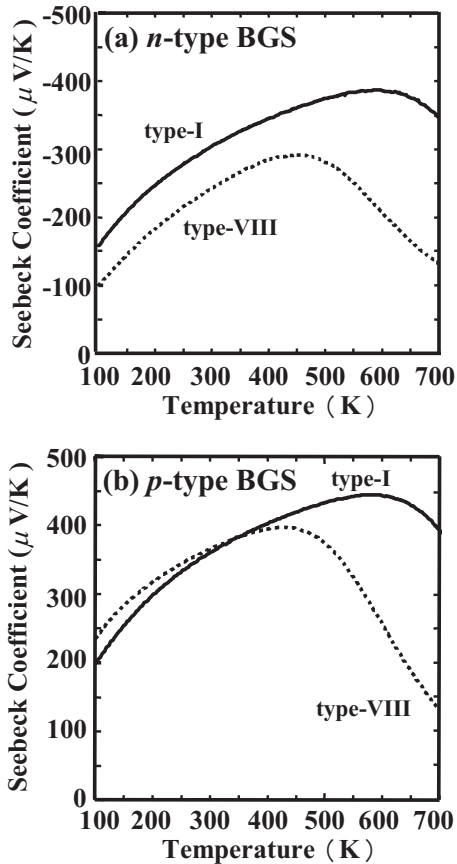


FIG. 5. Temperature dependence of calculated Seebeck coefficient at $n=1 \times 10^{19}/\text{cm}^3$: (a) *n*-type BGS, (b) *p*-type BGS.

Nos. 2 and 4, respectively. This trend is opposite in the experimental results. The reasons for this disagreement are not understood.

Figure 5 shows the calculated Seebeck coefficients of BGS-I and BGS-VIII as a function of temperature in a wide temperature range from 100 to 700 K. The carrier concentration was fixed at $1 \times 10^{19}/\text{cm}^3$. The decrease in absolute value of Seebeck coefficient at high temperatures is a feature of intrinsic semiconductors that is caused by the competition between opposite charged carriers: electrons and holes. Since the band gap for BGS-I (0.51 eV) is wider than that for BGS-VIII (0.32 eV), the maximum in the absolute value of Seebeck coefficient appears at a higher temperature for BGS-I than that of BGS-VIII.

n-type BGS-I has a higher Seebeck coefficient than *n*-type BGS-VIII, as shown in Fig. 5(a). The maximum absolute value of Seebeck coefficient is approximately

TABLE I. Estimated carrier concentrations in *n*-type BGS-I and BGS-VIII. The sample labels correspond to that in Fig. 4.

	This work (cm^{-3})	Expt. (cm^{-3}) ^a
BGS-I No. 1	2.0×10^{19}	3.8×10^{19}
BGS-I No. 2	6.4×10^{19}	3.4×10^{19}
BGS-VIII No. 3	1.0×10^{19}	3.2×10^{19}
BGS-VIII No. 4	4.0×10^{19}	1.0×10^{19}

^aReference 13.

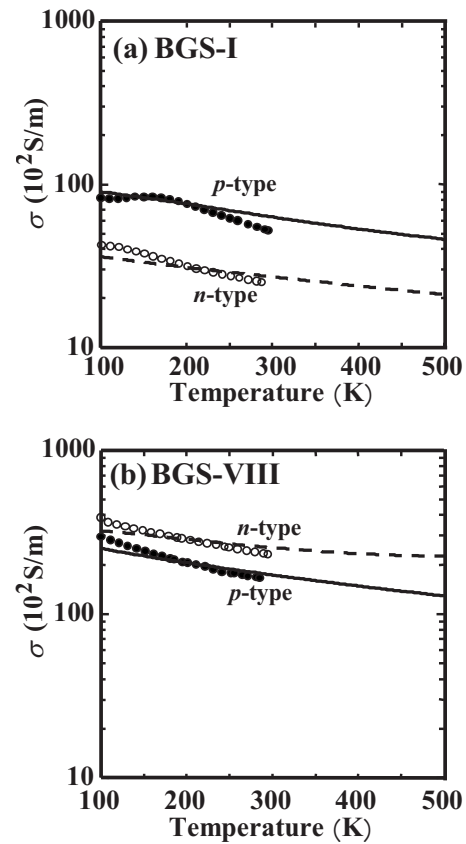


FIG. 6. Calculated electrical conductivity: (a) *n*-type and *p*-type BGS-I, (b) *n*-type and *p*-type BGS-VIII. Solid lines and dotted lines denote calculated results. Open circles and closed circles are experimental results (Ref. 13).

400 $\mu\text{V}/\text{K}$ at 600 K for BGS-I and 300 $\mu\text{V}/\text{K}$ at 460 K for BGS-VIII. In the present calculation, Seebeck coefficient depends only on the carrier concentration n and the electronic structure. As n was assumed to be $1.0 \times 10^{19}/\text{cm}^3$ for both BGS-I and BGS-VIII, the crystal structure dependence of Seebeck coefficient in Fig. 5 reflect the difference of the electronic structure. That is, the DOS near the band edge of the conduction band for BGS-I is steeper than that of BGS-VIII. In Fig. 5(b), the Seebeck coefficients of both types are similar in value until 350 K, above 350 K, Seebeck coefficient of BGS-VIII is strongly reduced. This behavior is reasonably understood from the DOS of the valence bands shown in Fig. 3(a).

The electrical conductivity σ was calculated using Eq. (2). The results are compared to the experimental results in Fig. 6. We fixed calculated electrical conductivity with the experimental result at 200 K. We obtained relaxation times as 1.2×10^{-16} s (*n*-type BGS-I), 6.9×10^{-17} s (*p*-type BGS-I), 4.2×10^{-16} s (*n*-type BGS-VIII) and 5.4×10^{-17} s (*p*-type BGS-VIII). The relaxation time of *n*-type BGS-VIII was longer than the others. This may be a result of the small mass of *n*-type carriers in BGS-VIII.

Figure 7 shows the estimated thermal conductivities $\kappa = \kappa_e + \kappa_l$ in the case of the carrier concentration $n=1 \times 10^{20}/\text{cm}^3$. The electronic thermal conductivity κ_e was calculated by using Eq. (3). The lattice thermal conductivity κ_l was assumed to be independent of temperature. The values

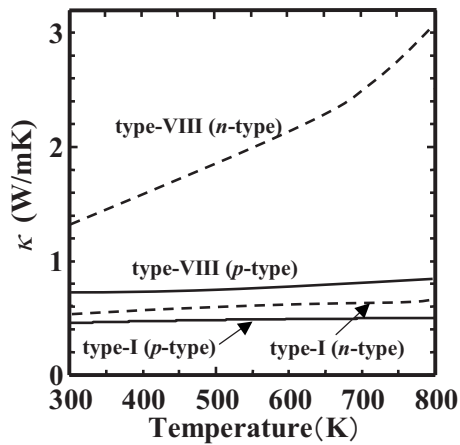


FIG. 7. Temperature dependence of thermal conductivities for *n*-type and *p*-type of BGS-I and BGS-VIII with the carrier concentration $n=1 \times 10^{20}/\text{cm}^3$.

of 0.38 W/mK and 0.66 W/mK were estimated for BGS-I and BGS-VIII, respectively, from our measurements at 300 K.

By using the values we calculated for Seebeck coefficient, electrical conductivity, and thermal conductivity, the figure of merit ZT can be calculated from Eq. (5). Figure 8 shows the calculated ZT for *n*-type BGS-VIII with three different values of carrier concentration. The calculated result is compared with the experimental ZT of the single crystalline sample with a carrier concentration of $2.1 \times 10^{19}/\text{cm}^3$ at 300 K. The experimental data agrees with the calculation for $n = 2.0 \times 10^{19}/\text{cm}^3$. At this carrier concentration, the maximum ZT is 0.8 and it does not exceed unity. It must be mentioned that the carrier concentration has not been optimized for high ZT yet. The figure of merit as a function of the carrier concentration for BGS-I and BGS-VIII at 700 K is shown in Fig. 9. For BGS-I, the maximum figure of merit reaches $ZT = 1.1$ for both *p*-type and *n*-type at the carrier concentration of $1.9 \times 10^{20}/\text{cm}^3$ (*p*-type) and $9.1 \times 10^{19}/\text{cm}^3$ (*n*-type). For BGS-VIII, on the other hand, the maximum ZT of *p*-type is 0.7 at $n = 2.0 \times 10^{20}/\text{cm}^3$, and that of *n*-type is 1.1 at $n = 9.1$

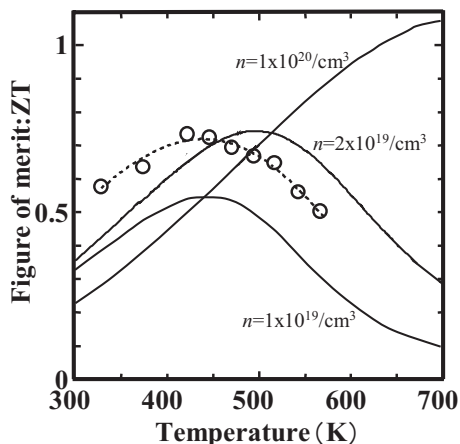


FIG. 8. Temperature dependence of figure of merit (ZT) for *n*-type BGS-VIII. Dotted line and open circles denote the experimental result. The calculated results are at three different carrier concentrations: $1 \times 10^{19}/\text{cm}^3$, $2 \times 10^{19}/\text{cm}^3$, and $1 \times 10^{20}/\text{cm}^3$.

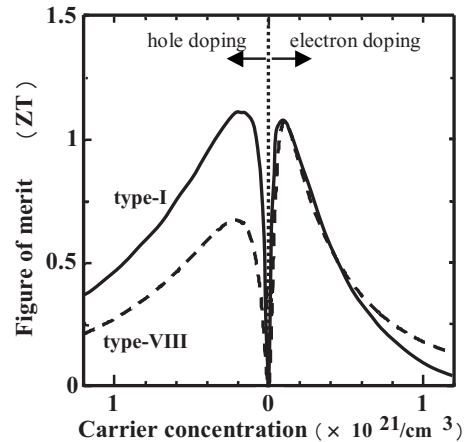


FIG. 9. Calculated figure of merit (ZT) as a function of carrier concentration for BGS-I (solid line) and BGS-VIII (dotted line) at 700 K.

$\times 10^{19}/\text{cm}^3$. The present calculations demonstrate that both *p*-type and *n*-type of BGS-I and *p*-type BGS-VIII have the potential of $ZT > 1$ if the carrier concentration is optimized.

IV. CONCLUSION

We calculated the electronic structure of clathrate compounds BGS-I and BGS-VIII by using first principle FLAPW method with EV-GGA. BGS-I and BGS-VIII were indirect semiconductors with the energy gaps of 0.51 eV and 0.32 eV, respectively. For BGS-I, the top of the valence band was relatively flat and the bottom of the conduction band was positioned at the M point. For BGS-VIII, the top of the valence band was positioned at the M point and the bottom of the conduction band was positioned at the Δ axis.

By using the calculated electronic structure, we calculated Seebeck coefficients, electrical conductivities, thermal conductivities, and figure of merits: ZT . The calculated Seebeck coefficients agreed well with experimental values. The absolute value of Seebeck coefficient of *n*-type BGS-I was larger than that of *n*-type BGS-VIII reflecting the band structure. However, the electrical conductivity of *n*-type BGS-I was lower than that of *n*-type BGS-VIII. As a consequence, both BGS-I and BGS-VIII with *n*-type carrier concentrations of $9.1 \times 10^{19}/\text{cm}^3$ showed almost the same figure of merit, $ZT = 1.1$ at 700 K. *p*-type BGS-I had higher figure of merit than *p*-type BGS-VIII because the former had lower thermal conductivity than the latter.

ACKNOWLEDGMENTS

The authors would like to acknowledge the PC cluster resources of the Media and Information Technology Center, Yamaguchi University, for the calculation of the electronic structure and thermoelectric properties. This work is partially supported by New Energy and Industrial Technology Development Organization (NEDO).

¹G. S. Nolas, J. L. Cohn, G. A. Slack, and S. B. Schujman, *Appl. Phys. Lett.* **73**, 178 (1998).

²J. L. Cohn, G. S. Nolas, V. Fessatidis, T. H. Metcalf, and G. A. Slack, *Phys. Rev. Lett.* **82**, 779 (1999).

³A. Saramat, G. Svensson, A. E. C. Palmqvist, C. Stiewe, E. Mueller, D. Platzek, S. G. K. Williams, D. M. Rowe, J. D. Bryan, and G. D. Stucky, *J.*

- Appl. Phys.* **99**, 023708 (2006).
- ⁴K. A. Kovnir and A. V. Shevelkov, *Russ. Chem. Rev.* **73**, 923 (2004).
- ⁵H. G. von Schnering, W. Carrillo-Cabrera, R. Kroner, E.-M. Peters, and K. Peters, *Z. Kristallogr. - New Cryst. Struct.* **213**, 679 (1998).
- ⁶B. Eisenmann, H. Schäfer, and A. Weiss, *J. Less-Common Met.* **118**, 43 (1986).
- ⁷W. Carrillo-Cabrera, R. Cardoso Gil, V.-H. Tran, and Y. Grin, *Z. Kristallogr. - New Cryst. Struct.* **217**, 181 (2002).
- ⁸V. L. Kuznetsov, L. A. Kuznetsova, A. E. Kaliazin, and D. M. Rowe, *J. Appl. Phys.* **87**, 7871 (2000).
- ⁹G. S. Nolas, J. L. Cohn, J. S. Dyck, C. Uher, G. A. Lamberton, Jr., and T. M. Tritt, *J. Mater. Res.* **19**, 3556 (2004).
- ¹⁰D. Huo, T. Sakata, T. Sasakawa, M. A. Avila, M. Tsubota, F. Iga, H. Fukuoka, S. Yamanaka, and T. Takabatake, *Phys. Rev. B* **71**, 075113 (2005).
- ¹¹M. A. Avila, K. Suekuni, K. Umeo, H. Fukuoka, S. Yamanaka, and T. Takabatake, *Phys. Rev. B* **74**, 125109 (2006).
- ¹²M. A. Avila, K. Suekuni, K. Umeo, H. Fukuoka, S. Yamanaka, and T. Takabatake, *Appl. Phys. Lett.* **92**, 041901 (2008).
- ¹³K. Suekuni, M. A. Avila, K. Umeo, H. Fukuoka, S. Yamanaka, T. Nakagawa, and T. Takabatake, *Phys. Rev. B* **77**, 235119 (2008).
- ¹⁴C. W. Myles, J. Dong, and O. F. Sankey, *Phys. Rev. B* **64**, 165202 (2001).
- ¹⁵T. F. Fässler, *Z. Anorg. Allg. Chem.* **624**, 569 (1998).
- ¹⁶L. Møllnitz, N. P. Blake, and H. Metiu, *J. Chem. Phys.* **117**, 1302 (2002).
- ¹⁷N. P. Blake, S. Lattner, J. D. Bryan, G. D. Stucky, and H. Metiu, *J. Chem. Phys.* **115**, 8060 (2001).
- ¹⁸Y. Li, J. Gao, N. Chen, Y. Liu, Z. P. Luo, R. H. Zhang, X. Q. Ma, and G. H. Cao, *Physica B* **403**, 1140 (2008).
- ¹⁹K. Koga, T. Kamei, K. Akai, K. Oshiro, and M. Matsuura, in Proceedings of 24th International Conference on Thermoelectrics, Clemson, USA, p. 207 (2005).
- ²⁰P. Blaha, K. Schwarz, G. Madsen, D. Kvasnicka and J. Luitz, program package WIEN2K, Technical University of Vienna (2001).
- ²¹E. Engel and S. H. Vosko, *Phys. Rev. B* **47**, 13164 (1993).
- ²²N. P. Blake, J. D. Bryan, S. Lattner, L. Møllnitz, G. D. Stucky, and H. Metiu, *J. Chem. Phys.* **114**, 10063 (2001).
- ²³T. Uemura, K. Koga, K. Akai, and M. Matsuura, *Trans. Mater. Res. Soc. Jpn.* **312**, 311 (2006).